nature COMMUNICATIONS

ARTICLE

Received 17 Dec 2012 | Accepted 5 Jul 2013 | Published 5 Aug 2013

DOI: 10.1038/ncomms3254 OPEN

Noise-resilient quantum evolution steered by dynamical decoupling

Gang-Qin Liu[1,*], Hoi Chun Po[2,*], Jiangfeng Du[3], Ren-Bao Liu[2,4,5] & Xin-Yu Pan[1]

Realistic quantum computing is subject to noise. Therefore, an important frontier in quantum computing is to implement noise-resilient quantum control over qubits. At the same time, dynamical decoupling can protect the coherence of qubits. Here we demonstrate non-trivial quantum evolution steered by dynamical decoupling control, which simultaneously suppresses noise effects. We design and implement a self-protected controlled-NOT gate on the electron spin of a nitrogen-vacancy centre and a nearby carbon-13 nuclear spin in diamond at room temperature, by employing an engineered dynamical decoupling control on the electron spin. Final state fidelity of 0.91(1) is observed in preparation of a Bell state using the gate. At the same time, the qubit coherence time is elongated at least 30 fold. The design scheme does not require the dynamical decoupling control to commute with the qubit interaction and therefore works for general qubit systems. This work marks a step towards implementing realistic quantum computing systems.

[1] Beijing National Laboratory for Condensed Matter Physics and Institute of Physics, Chinese Academy of Sciences, Beijing 100190, China. [2] Department of Physics, The Chinese University of Hong Kong, Shatin, New Territories, Hong Kong, China. [3] Hefei National Laboratory for Physical Sciences, Microscale and Department of Modern Physics, University of Science and Technology of China, Hefei, Anhui 230026, China. [4] Centre for Quantum Coherence, The Chinese University of Hong Kong, Shatin, New Territories, Hong Kong, China. [5] Institute of Theoretical Physics, The Chinese University of Hong Kong, Shatin, New Territories, Hong Kong, China. * These authors contributed equally to this work. Correspondence and requests for materials should be addressed to R.-B.L. (email: rbliu@phy.cuhk.edu.hk) or to X.-Y.P. (email: xypan@aphy.iphy.ac.cn).

To combat noise effects in quantum computing, there are three main strategies, namely, quantum error corrections[1–3], decoherence-free subspace[4,5] and dynamical decoupling (DD)[6–9]. DD, which originated from magnetic resonance spectroscopy, can average out the noise by flipping the qubit. DD has the merits of requiring no extra qubits and potential compatibility with quantum gates. It provides a potential method to realize fidelity of quantum gates above the threshold required by concatenated quantum error corrections for scalable fault-tolerant quantum computing[1–3]. Recent experiments have demonstrated the preservation of quantum coherence[10–15], or the NULL gate in terminology of quantum computing.

Integration of DD with quantum gates, however, is a non-trivial challenge because, in general, the quantum gates may not commute with the DD control and therefore can interfere with the DD. A straightforward approach is to insert the quantum gates in between the DD control sequences[16,17], which, however, significantly reduces the time windows for quantum gates. A clever solution is to design the DD sequences such that they commute with the qubit interaction, which can be realized either by encoding the qubits in decoherence-free subspaces[18] or by choosing a certain qubit interaction that commutes with the DD sequences[19]. It is also possible to apply control over one qubit while the other qubits are under DD control[20–22]. These methods, however, require special types of interactions or hybridizing operations at very different timescales.

A more important question is whether DD, instead of locking the quantum states of qubits as previously demonstrated[10–14], can steer non-trivial and noise-resilient quantum evolutions of qubits with generic interactions (that is, not limited to interactions commutable with the DD control)[23]. Recent theoretical studies established that arbitrarily accurate dynamical control could be designed for general quantum open systems via concatenated construction or pulse shaping[24,25].

Here we demonstrate the feasibility of integrating DD with quantum gates by steering the quantum evolution of a hybrid qubit system with numerically optimized DD control, to simultaneously realize a non-trivial two-qubit gate and coherence protection. We realize a self-protected controlled-NOT (C_eNOT_n) gate on the electron spin of a nitrogen-vacancy (NV) centre and a nearby carbon-13 nuclear spin in diamond, by employing an engineered DD control applied only on the electron spin.

Results

Design of quantum gates by DD. To demonstrate the concept of quantum steering by DD, we consider a negatively charged NV centre in a type IIa diamond (with nitrogen concentration <10 ppb) under an external magnetic field **B**. The scheme is motivated by the recent study of central spin decoherence in nuclear spin baths[26–30], which reveals that because of the quantum nature of the qubit-bath coupling, the quantum evolution of nuclear spins is actively manipulated by flipping the central electron spin. Such quantum nature of qubit-bath coupling has been previously utilized to realize control of nuclear spins by flipping the electron spin[31–34]. By engineering the timing of the electron spin flipping, one can steer a noise-resilient quantum evolution of interacting qubits simply by DD control. Recent research on single nuclear spin sensing by central spin decoherence[33,35–39] has already demonstrated the quantum nature of coupling between a NV centre spin and remote nuclear spins, and therefore the approach of quantum gates by DD may also be applied to those remote nuclear spins and this has the potential of extending the two-qubit system to few-qubit systems.

The NV centre electron spin is coupled through hyperfine interaction to ^{13}C nuclear spins[40], which have a natural abundance of 1.1% (Fig. 1a). Lifting the degeneracy between $m=+1$ and $m=-1$ NV centre spin states by **B**, we encode the first qubit in the centre spin states $|0\rangle\equiv|m=0\rangle$ and $|1\rangle\equiv|m=-1\rangle$. As the hyperfine interaction strength decreases rapidly with the distance between a nuclear spin and the NV centre, a proximal ^{13}C spin can be identified by its strong hyperfine splitting in the optically detected magnetic resonance (ODMR) spectra. We encode another qubit in the ^{13}C nuclear spin-1/2 states $|\uparrow\rangle$ and $|\downarrow\rangle$ (Fig. 1b), similar to the electron-nuclear spin register studied in Gurudev Dutt *et al.*[33] Thus, we have a well-defined two-qubit system.

The undesired coupling of this two-qubit system to the other ^{13}C spins in the bath leads to loss of quantum information and therefore reduces the fidelity of the quantum operations. In particular, because of the large difference between the gyromagnetic ratios of the two types of spins, the electron spin decoherence occurs in a timescale that is shorter than the typical operation timescale of the nuclear spin qubit, which results in difficulty in realizing high-fidelity two-qubit operations.

The evolution of the two-qubit system is a path in the curved SU(4) operator space[41]. In a free evolution, the system propagator

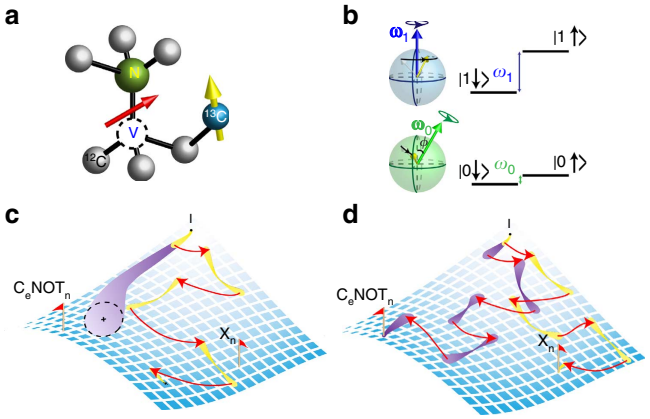

Figure 1 | System and approach for steering quantum evolution by DD. (**a**) The electron-nuclear spin qubit system. The NV centre electron spin (electron qubit) is coupled to a bath of nuclear spins in a high purity diamond, and a proximal ^{13}C nuclear spin (nuclear qubit) is identified by a stronger hyperfine coupling. (**b**) The conditional local field experienced by the nuclear spin. Because of its coupling with the centre spin, both the quantization axis and the precession rate of the nuclear spin depend on the state of the centre spin. (**c**,**d**) Quantum evolution in the operator space, starting from the identity operator I. Under a free evolution (yellow and purple path bundles), the propagator follows the natural 'landscape' of the curved operator space. A stroboscopic control (the red arrows) moves the operator to a new position. (**c**) Propagator evolution in the conventional settings. In a FID experiment (purple path), the coupling between the system and the bath causes non-ideal evolution of the system propagator, and therefore the path of the propagator spreads out in the operator space. In a conventional Carr-Purcell-Meiboom-Gill sequence (yellow path), π-pulses (red arrows) are applied at designed intervals to decouple the system from the environment and can therefore refocus the uncertainty in the system propagator. Yet, in both cases, the quantum dynamics of the system is unconstrained and, in general, the resultant propagator is not the target one. (**d**) Steering quantum evolution by DD. In contrast to the conventional schemes, one can relax the timing constraint in applying the DD π-pulses and thereby steer the system propagator to the desired points in the operator space. For instance, the C_eNOT_n and the nuclear qubit Pauli-X (X_n) gates can be realized by the purple and the yellow paths, respectively, by tuning the timing parameters in the four-pulse DD sequence.

follows the natural landscape in the operator space, but the uncertainty in the system propagator increases with time due to the coupling with the environment (Fig. 1c). Although a conventional DD scheme like the Carr-Purcell-Meiboom-Gill sequence or the Uhrig DD sequence can efficiently refocus the otherwise non-coherent evolution of the system propagator, the sequence in general corresponds to an unspecified two-qubit propagator unless resonant values of the total evolution time and the number of pulses are chosen[21,38] or additional manipulation on the nuclear spin is employed[21]. Simultaneously achieving coherence protection and gate implementation, our scheme can be intuitively understood as a systematic approach to identify a path in the operator space comprising segments of free evolution and centre spin π-flips such that the path is self-protected and guided from the identity to a desired two-qubit gate (Fig. 1d).

Because the timescale of interest is much shorter than the longitudinal relaxation time of the centre spin, the centre spin magnetic number m remains a good quantum number and the Hamiltonian of the two-qubit system can be expanded in the basis of the centre spin eigenstates $|0\rangle$ and $|1\rangle$ (Supplementary Note 1), given by $H=\sum_m |m\rangle\langle m|(E_m+\boldsymbol{\omega}_m\cdot\mathbf{I})=\sum_m |m\rangle\langle m|h_m$, where E_m is the eigen-energy of the centre spin state $|m\rangle$, $\mathbf{I}$ represents the nuclear spin and $\boldsymbol{\omega}_m$ is the local field for the nuclear spin conditioned on the electron spin state $|m\rangle$. In general, when the centre spin state is altered, the nuclear spin will evolve under a different local field, and therefore the nuclear spin evolution is conditional on the state of the centre spin[33,34,37,40–44]. When the angle ϕ between $\boldsymbol{\omega}_1$ and $\boldsymbol{\omega}_0$ is non-zero (Fig. 1b), which is expected in a general setting (Supplementary Note 1), they represent different axes on the nuclear spin Bloch sphere and hence can be utilized to generate universal qubit operations conditioned on the electron spin qubit.

To be specific, we suppose the system is prepared in an initial state $|\Psi\rangle=\sum_m |m\rangle|\psi_m\rangle$. When a sequence of N π-pulses is applied to the centre spin, the nuclear spin state $|\psi_m\rangle$ evolves to $|\psi_m'\rangle=u_m\{t_\alpha\}|\psi_m\rangle$ with $u_0\{t_\alpha\}=e^{-ih_\sigma t_N}\ldots e^{-ih_0 t_2}e^{-ih_1 t_1}e^{-ih_0 t_0}$, where t_α is the time between the α-th and the $(\alpha+1)$-th pulses, $\sigma=0$ for N being even and $\sigma=1$ for N being odd, and $u_1\{t_\alpha\}$ is similarly defined. This implies that the system propagator can be represented by $U\{t_\alpha\}=\sum_m |m\rangle\langle m|\otimes u_m\{t_\alpha\}$. One can vary the timing parameters $\{t_\alpha\}$ and engineer the system evolution such that $U\{t_\alpha\}\approx G$ for some desired two-qubit gates with the generic form $G=\sum_m |m\rangle\langle m|\otimes O_m$, where O_m's are nuclear spin operators. Important examples of gates with this form include the C_eNOT_n gate, nuclear spin single-qubit gates, centre spin phase gates and the two-qubit NULL gate. In general, it is non-trivial to exactly solve $u_m\{t_\alpha\}=O_m$ because of the nonlinearity and the large number of variables in the problem. Yet, one can recast the design protocol into a maximization problem through studying the average two-qubit gate fidelity $\overline{F}\{t_\alpha\}=\int d\Psi\,\mathrm{Tr}(U\{t_\alpha\}|\Psi\rangle\langle\Psi|U^\dagger\{t_\alpha\}G|\Psi\rangle\langle\Psi|G^\dagger)$, where $|\Psi\rangle$ is a general pure two-qubit state and the integration is over the normalized uniform measure of the state space[45]. As $\overline{F}\{t_\alpha\}=1$ if and only if $U\{t_\alpha\}=G$, the gate G is simulated by the system propagator when the timing parameters $\{t_\alpha\}$ are chosen to maximize $\overline{F}\{t_\alpha\}$. Such gate design can be achieved by using only DD sequences, where the notion of DD can be understood as a set of criteria on the timing parameters $\{t_\alpha\}$ between the centre spin π-pulses. Although a conventional N-pulse DD sequence (say the Carr-Purcell-Meiboom-Gill sequence) is characterized by just one timing parameter, namely the pulse delay time, the general DD criteria can be derived by studying the expansion of the coherence function. Instead of using all the timing parameters to optimize protection of the centre spin coherence[46], one can relax some of the timing parameters by reducing the decoherence suppression order. The design procedure can be summarized as the maximization of $[F\{t_\alpha\}]$ with respect to an N-pulse sequence $\{t_\alpha\}$ that complies with a set of DD constraints. The first order DD criterion requires $t_0-t_1+t_2+\cdots+(-1)^N t_N=0$, which can be intuitively understood as the spin echo condition. The symmetric timing condition $t_n=t_{N-n}$ automatically realizes the second-order DD[47,48], and higher-order DD criteria can be similarly introduced. At least up to the second order, the DD constraints discussed above are independent of the detailed bath spectrum. DD constraints to higher orders may also be designed independent of the detailed noise spectrum, but a hard high-frequency cut-off (that is, slow noises) is required.

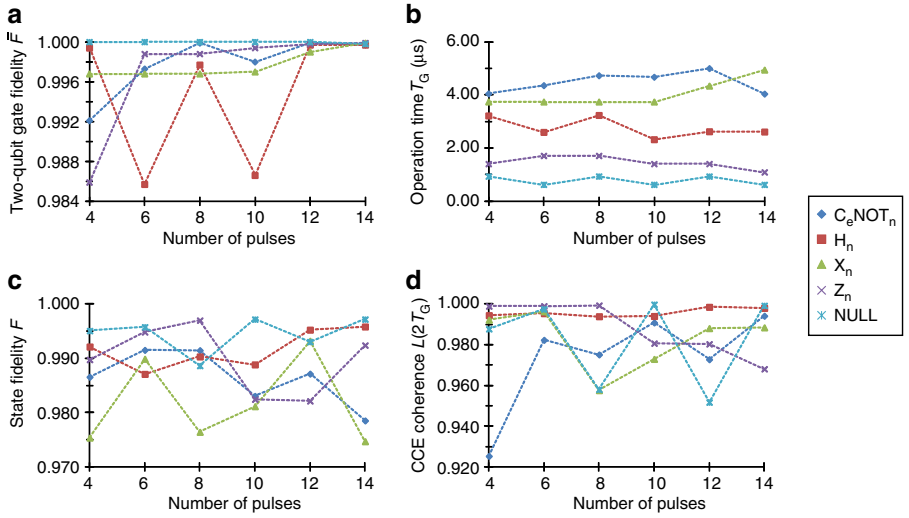

Figure 2 | Simulation of two-qubit gates by DD. By varying the timing parameters in the DD sequences with different numbers of pulses, five two-qubit gates were designed (Supplementary Table S1) and studied numerically, namely, the C_eNOT_n gate, nuclear qubit Hadamard (H_n), Pauli-X (X_n) and Pauli-Z (Z_n) gates, and the two-qubit NULL gate. The dotted lines are guides to the eye. (**a**) Ideal gate fidelities of the five gates from sequence optimization (no decoherence included). The maximized fidelity approaches to unity when the number of pulses increases to 14. (**b**) Operation times of the gates as designed in **a** as functions of the number of pulses. (**c**) State fidelities evaluated by exact diagonalization of a small bath. Although in general a high fidelity is achieved, the fidelities, in contrast to the optimized ideal fidelities in **a**, do not increase monotonically with the number of pulses. (**d**) Coherence function probed after applying the gate twice as a function of the number of pulses.

As a demonstration of principles, we used the echo condition and the symmetric requirement to realize the DD to the second order[47,48]. The DD constraints are explicitly in the form $\{t_\alpha\}_{DD} = \{t_0,t_1,t_2,\ldots t_2,t_1,t_0\}$ with the echo condition $\sum_\alpha (-1)^\alpha t_\alpha = 0$. With such, we designed DD sequences that execute the desired two-qubit gates by maximizing $\bar{F}\{t_\alpha\}_{DD}$ with respect to the N-independent timing variables. It is straightforward to generalize the design to higher-order DD for better noise resilience.

We demonstrate the feasibility of the design by considering an experimentally identified target ^{13}C spin coupled to an NV centre spin. The experimental parameters were extracted from the ODMR spectra of the NV centre and the free precession signal of the nuclear spin, which were $\omega_0 = 0.256(2)$ MHz and $\omega_1 = 6.410(2)$ MHz (see Methods and Supplementary Fig. S1 for details). The magnetic field **B** was oriented such that ϕ was 90°.

Various DD gate sequences in Supplementary Table S1, were designed based upon the obtained experimental parameters, and their performances were assessed numerically (Fig. 2a–d). Five different two-qubit gates, namely, the C_eNOT_n gate (defined up to an additional $\pi/2$ phase shift of the centre spin)[21], the nuclear spin Hadamard (H_n), Pauli-X (X_n) and Pauli-Z (Z_n) gates, and the two-qubit NULL gate, were designed using sequences with 4–14 pulses. The gate fidelity $\bar{F}\{t_\alpha\}$ (ref. 45), numerically optimized, is at least 0.98 for the gates we considered, and the gate operation time T_G ranges from 1.4 to 5 μs. To incorporate the coupling between the two-qubit system and the environment, we simulated the environment by a small bath consisting of six ^{13}C spins aside from the ^{13}C qubit spin. The coupling to the spin bath causes centre spin decoherence in a timescale of $T_2^* \approx 1.6(1)$ μs under free induction decay (FID), which is consistent with the experimental condition. To characterize the performance of the designed gates (G), we considered a typical system initial state $|\Psi_0\rangle = \frac{1}{\sqrt{2}}(|0\downarrow\rangle + |1\downarrow\rangle)$ and the bath in the thermal state ρ_{bath}. We then calculated the total propagator U_T under the pulse sequences by exact diagonalization, assuming perfect π-pulses and inter-pulse timing. The state fidelity F is defined by $F = \sqrt{\langle\Psi_i|\rho_s|\Psi_i\rangle}$ (ref. 42), where $|\Psi_i\rangle = G|\Psi_0\rangle$ is the ideal system final state and $\rho_s = \mathrm{Tr}_{bath}(U_T(|\Psi_0\rangle\langle\Psi_0| \otimes \rho_{bath})U_T^\dagger)$ is the simulated system density matrix. We found the final state fidelity to be at least 0.97 for the sequences we designed. We also characterized the coherence protection efficacy of the DD gate sequences by performing the cluster-correlation expansion calculation[43] with a larger bath of 44 ^{13}C spins together with the ^{14}N nitrogen spin. Because of entanglement with the target spin, the centre spin coherence right after applying the DD gate sequence can be 0. For a fair comparison, therefore, we probe the

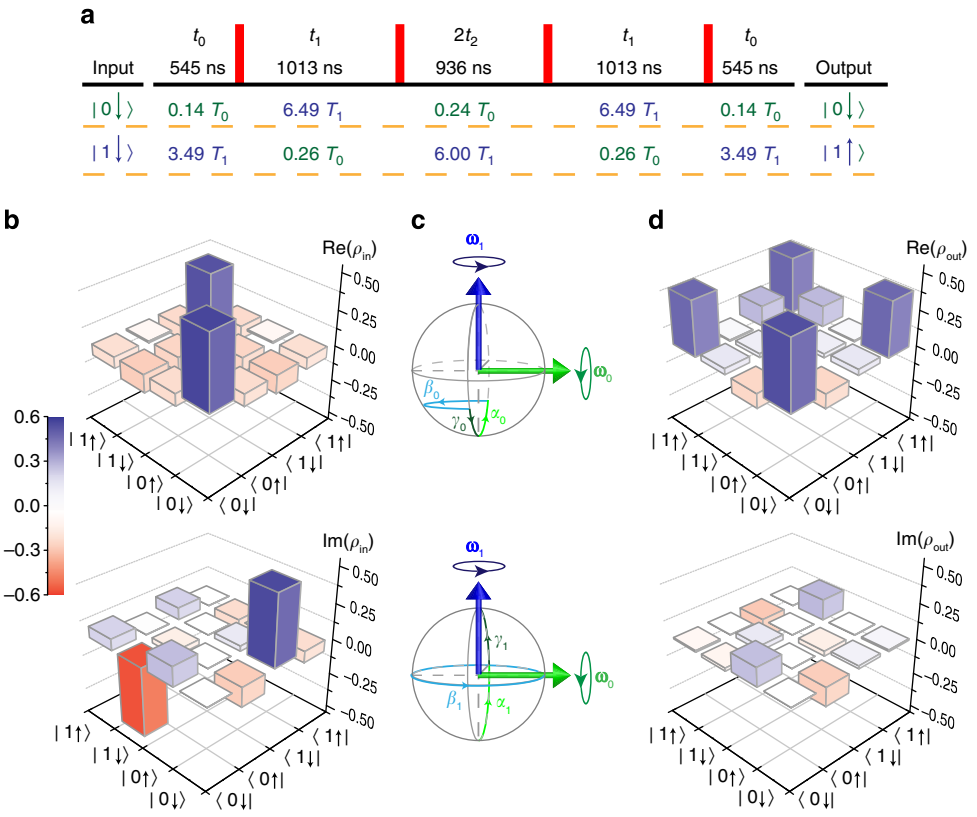

Figure 3 | Implementing the C_eNOT_n by DD. The effect of the gate is studied by performing state tomography on the system before and after the gate. (**a**) The DD pulse sequence for realizing the C_eNOT_n gate. The numbers in the first line indicate the time intervals between the flips of the NV centre spin, and the numbers in the second and third lines are the intervals in units of $T_0 \equiv 2\pi/\omega_0$ (green) or $T_1 \equiv 2\pi/\omega_1$ (blue), the precession periods of the nuclear qubit for the electron qubit in the $|0\rangle$ or $|1\rangle$ state. (**b**) State tomography for the initial state $(1/\sqrt{2})(|0\downarrow\rangle - i,|1\downarrow\rangle)$. The bars are coloured according to the corresponding entries in the measured density matrices, with blue and red representing positive and negative values, respectively. (**c**) Schematic of the conditional evolution of the $|0\downarrow\rangle$ (upper panel) and $|1\downarrow\rangle$ (lower panel) states steered by the DD. The conditional quantization axes of the nuclear qubit, $\boldsymbol{\omega}_0$ and $\boldsymbol{\omega}_1$ are represented by green and blue arrows, respectively. With $|0\downarrow\rangle$, the nuclear spin first precesses about $\boldsymbol{\omega}_0$ and alternates between $\boldsymbol{\omega}_0$ and $\boldsymbol{\omega}_1$ under the DD gate sequence. The nuclear qubit traces out the path $\alpha_0 - \beta_0 - (\gamma_0 + \alpha_0) - \beta_0 - \gamma_0$ under the sequence $t_0 - t_1 - (t_2 + t_2) - t_1 - t_0$ and returns to the original state at the end of the sequence. For $|1\downarrow\rangle$, the nuclear spin first precesses about $\boldsymbol{\omega}_1$ for t_0. It then evolves during $t_1 - 2t_2 - t_1$ along the path $\alpha_1 - \beta_1 - \gamma_1$ and is hence flipped. (**d**) State tomography of the output Bell state for the initial state in **b** (same colour scale). The resultant state fidelity is measured to be 0.91(1).

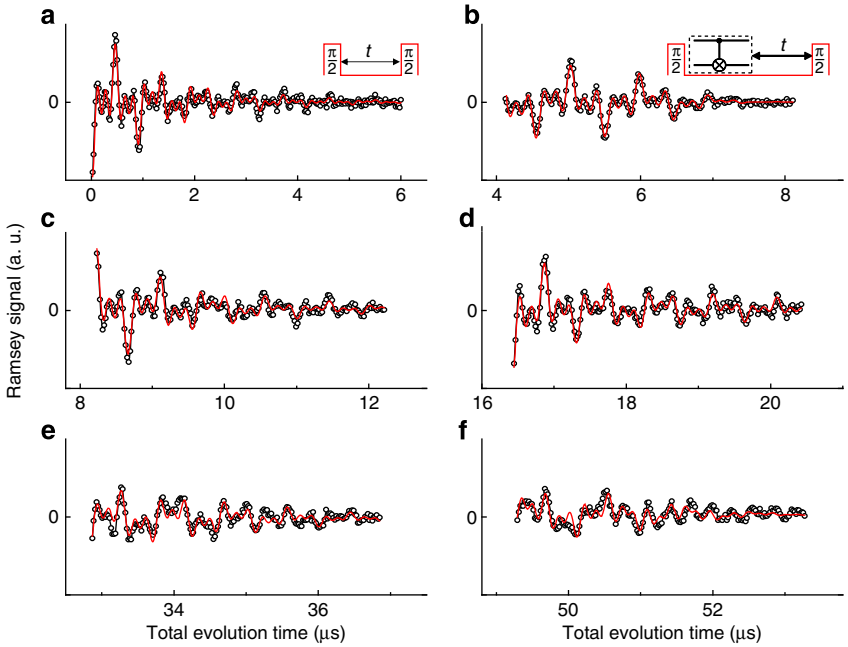

Figure 4 | Coherence protection by the DD gate sequence. The signals were measured by Ramsey interference before or after the DD control. The symbols are experimental data, and the red lines are fittings to decay envelopes modulated by cosine functions. (**a**) Centre spin coherence in free-induction decay without applying the designed gate (pulse sequence shown in the inset). The coherence is lost in $T_2^* \approx 1.6(1)\,\mu s$. (**b**) Centre spin coherence after applying the DD gate sequence (shown in inset). Right after the DD gate sequence the centre spin coherence is 0, which is expected due to the maximum entanglement between the electron and the nuclear qubits by the C_eNOT_n gate. The strong revival peaks in the Ramsey interference signal after implementing the DD gate indicates that the centre spin coherence is well protected. (**c**–**f**) The centre spin coherence after the DD gate sequence is repeated for $N = 2$, 4, 8 and 12 times from **c** to **f**. Strong interference oscillations are observed in all cases, which indicates that the coherence time is elongated from T_2^* by at least 30 fold.

centre spin coherence $L(t)$ (ref. 44) after performing each gate sequence twice, such that ideally one would obtain $L(2T_G) = 1$ for the gates we considered. The coherence function was found to be at least 0.92 even when the total evolution time exceeds the FID decoherence timescale. We note that although in principle the average two-qubit gate fidelity can be improved to almost unity by using a larger number of pulses, this does not automatically guarantee a higher resultant state fidelity when the spin bath is incorporated, and in the experimental setting, this can also introduce additional pulse errors.

As the gates realized by applying DD sequences are self-protected, our method offers an integrated solution to achieving both control and noise tolerance in quantum information processing. We note that when the hyperfine interaction is moderately strong, the gate speed of the nuclear spin gates constructed this way can be significantly faster than the conventional control by radio frequency pulses[31,32].

Experimental implementation. We experimentally demonstrated our scheme by implementing the designed four-pulse C_eNOT_n gate (Fig. 3a). Because the nuclear spin of the nitrogen host was not polarized in the experiment, the system was first initialized into the superposition state $\frac{1}{\sqrt{2}}(|0\downarrow\rangle - i|1\downarrow\rangle)$ within the $m_I = 0$ subspace of the ^{14}N spin using selective weak microwave (MW) pulses. We used state tomography to measure the state fidelity, which is defined as $\sqrt{\langle\Psi_i|\rho_E|\Psi_i\rangle}$ with $|\Psi_i\rangle$ being the ideal state of the system and ρ_E being the measured reduced density matrix[42]. The measured initial state fidelity was 0.99(1) (Fig. 3b). The particular gate demonstrated can be readily understood by studying the state trajectory on the Bloch sphere. As illustrated in Fig. 3c, the nuclear qubit traces out paths that would approximately leave it unchanged or flipped when the centre spin is prepared in the $|0\rangle$ or $|1\rangle$ states, respectively. State tomography revealed that the nuclear spin was flipped conditional to the state of the centre spin and the final state resembled the Bell state $\frac{1}{\sqrt{2}}(|0\downarrow\rangle + |1\uparrow\rangle)$ with fidelity of 0.91(1) (Fig. 3d). We also carried out experiments for the system initially prepared in the basis states. The final state fidelity, as shown in Supplementary Fig. S2, ranged from 0.86(1) to 0.93(1).

Having demonstrated the quantum gate aspect of the sequence, we now turn to illustrate the coherence protection aspect of our design by applying the C_eNOT_n gate DD sequence to an initial superposition state $|\Psi_0\rangle = \frac{1}{\sqrt{2}}(|0\downarrow\rangle - i|1\downarrow\rangle)$ using stronger selective MW pulses that drive all the components of the ^{14}N spin. Without coherence protection, the electron spin coherence decays in a short time of $T_2^* \approx 1.6(1)\,\mu s$ in FID, and the coherence was completely lost in $\sim 2\,\mu s$ (Fig. 4a). With the DD gate sequence, however, the centre spin coherence was well protected during the course of gate operation, even though the duration of the gate was more than twice of T_2^* (Fig. 4b). The coherence protection capacity of the DD gate sequence is further illustrated in Fig. 4c–f. The designed pulse sequence was repeated for $N = 2$, 4, 8 and 12 times on the initial state $|\Psi_0\rangle$, and the Ramsey interference signal was measured after the total sequence time of 8, 16, 32 and 48 μs, correspondingly. The presence of strong coherent oscillation after an interval longer than 30 times of T_2^* demonstrates the robust protection effect of the DD gate design.

Discussion

Although the scheme was designed and implemented for a specific system with interaction diagonal in the electron spin qubit basis, the design protocol of optimizing gate fidelity under

the DD constraints can be applied to general systems provided that (1) the qubits are well defined with respect to the bath, (2) at least one of the qubits can be independently controlled by DD pulses and (3) the bath dynamics is slow as compared with the control and the inter-qubit interactions or the noise spectrum has a hard high-frequency cut-off. In principle, all quantum gates that are allowed by the inter-qubit interactions can be designed. Let us consider, for instance, a p-qubit system with general inter-qubit interactions characterized by the system Hamiltonian H_p. When a total of N DD pulses are applied to more than one qubits, the system propagator is given by $U_p\{t_\alpha, q_\alpha\} = e^{-iH_p t_N}\sigma^x_{q_N} \ldots \sigma^x_{q_2} e^{-iH_p t_1}\sigma^x_{q_1} e^{-iH_p t_0}$, where $\{t_\alpha\}$ specifies the inter-pulse timings and $\{q_\alpha\}$ specifies the qubit that the α-th DD pulse flips. The gate fidelity can then be maximized with respect to both $\{t_\alpha\}$ and $\{q_\alpha\}$ subjected to the DD constraints. Alternatively, one may also apply DD pulses to only one qubit and derive DD constraints that can protect the coherence of the multi-qubit system[49]. To combat general qubit-bath coupling (beyond the pure dephasing model), the qubit flips along different axes (such as $\sigma^y_{q_\alpha}$ and $\sigma^z_{q_\alpha}$) can be employed.

It should be noted that when the system is too large, the numerical optimization procedure can become intractable as the gate fidelity has to be maximized with respect to the high-dimension system propagators over the large parameter space, and the numerical complexity increases exponentially with the number of qubits in the system[24]. A set of one- and two-qubit gates is sufficient for universal quantum computing. For multiple qubits coupled to common noise sources, however, collective design of multiple-qubit control would still be needed. Given a realistic limitation on numerical resources, the achievable fidelities of the multiple-qubit control would drop due to the exhaustion of optimization parameters. Such a limitation is a common issue for all numerical optimization schemes for noise-resilient qubit control. On the other hand, because the DD constraints depend only on the algebraic form of qubit-bath couplings but not on the qubit–qubit couplings, the coherence protection capacity of the scheme should not suffer from a growth in the system size.

Although the gate-by-DD scheme demonstrated in this work is based on optimization of a discrete set of timing parameters, we note that numerical pulse shaping has been proposed for dynamically protected quantum gates, in which both environmental noise and control errors can be corrected[25]. In this paper, we have not considered the effects of control errors (which is actually the main source of infidelity in our experimental implementation). The gate-by-DD scheme, however, can also be extended to employ robust DD sequences[50] for tolerance of control errors. As the DD gate design does not depend on the phase of the DD pulses, the scheme can be extended to employ both X and Y DD pulses so as to protect the gates against pulse imperfection[50].

This work demonstrates a general approach to quantum information processing in which the quantum evolution of the system is engineered to perform decoupling from a large spin bath and execute a designated gate on the two-qubit system, and thereby simultaneously realize high-fidelity two-qubit gates and coherence protection. The approach developed here is applicable to other systems under a general setting and therefore provides a new avenue towards achieving scalable and fault-tolerant quantum computing.

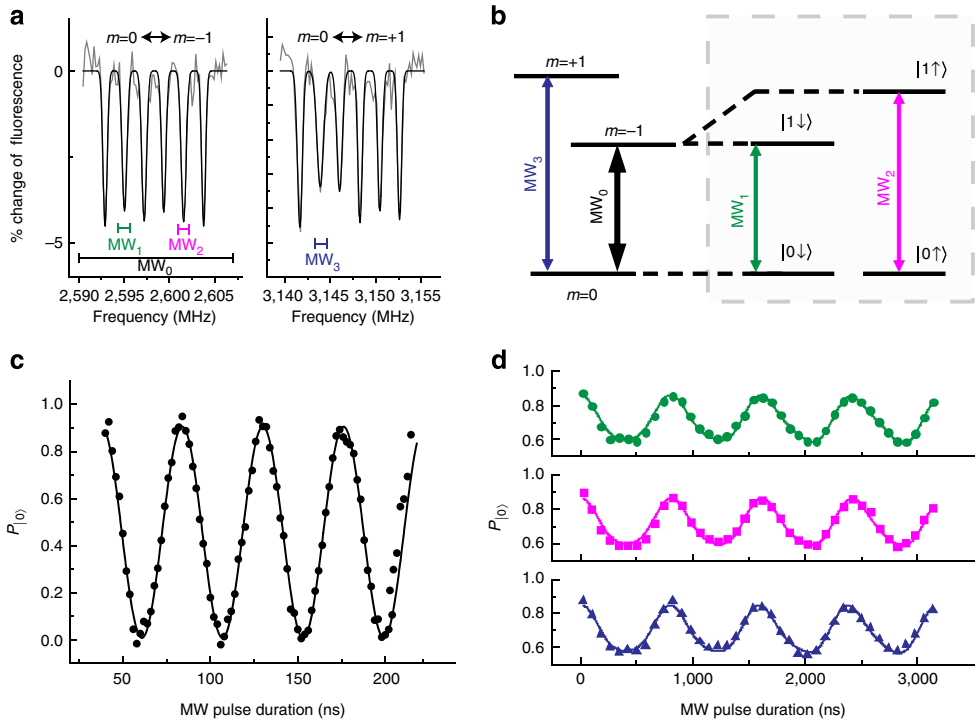

Figure 5 | System characterization and control. (**a**) Pulsed ODMR spectra of the NV centre under study. The signal is fitted to Gaussian line shapes. Other than the splitting due to the ^{14}N nuclear spin, the hyperfine splitting due to a strongly coupled proximal ^{13}C spin was resolved, which allows isolation of this spin from the bath to form a nuclear spin qubit. (**b**) Energy level diagram of the system and the resonant frequencies of the different MW pulses used. (**c**,**d**) Rabi oscillations driven by different MW channels. $P_{|0\rangle}$ denotes the population in the $|0\rangle$ state. (**c**) Full Rabi oscillation between the centre spin $m=0$ and $m=-1$ states was driven by the strong MW_0 pulse. The symbols are experimental data, and the line is fitting to a cosine function. (**d**) Selective Rabi oscillations between different states were driven by the weak MW_1 (green), MW_2 (magenta) and MW_3 (blue) pulses. The signals are each fitted to a superstition of two cosine functions corresponding to the in- and off-resonance oscillations. Note that the selective Rabi oscillations drove only one-third of the $m=0$ population, as weaker MW pulses were used such that the ^{13}C spin was polarized only in the $m_I=0$ subspace.

Methods

Experimental setup. A permanent magnet was used to apply an external magnetic field on the system such that the field **B** can be tuned in both strength (0–650 Gauss) and orientation. A home-built scanning confocal microscope combined with integrated MW devices was employed to initialize, control and read out the electron spin state. The 532-nm continuous wave laser beam was switched on and off by an acoustic optical modulator, and the position of the laser spot was controlled by an X-Y galvanometer before the beam was directed to the sample through an oil immersion lens. The spin state-dependent fluorescence of the NV centre was collected by the same lens and filtered by a 532-nm notch and a 650-nm long path. Then, the weak light signal was translated into the electronic pulse signal by a single-photon counting module and was subsequently counted by a pulse counter.

A total of four MW channels were time-controlled by individual RF switches and were then combined and amplified by a 16-Watt wide-band MW amplifier before being delivered to the sample through a coplanar waveguide antenna close to the NV centre. One of the MW channels was used to execute the DD gate sequences in our scheme, and the others were used for the polarization and readout procedures.

The timing sequences for controlling the acoustic optical modulator, RF switches and counter were generated by a multi-channel pulse generation card (with 2 ns resolution). In each of the measurement, we loaded the pulse sequence to the card memory, and other instruments were triggered and controlled by the generated digital logic signal. The sequence was repeated (typically for 400,000 times) until a reliable signal-to-noise ratio was reached.

System characterization and control. The energy splittings between different levels were first measured using the pulsed ODMR technique (Fig. 5a). MW pulses of various powers, frequencies and phases were employed to coherently control the NV centre electron spin (Fig. 5b). Figure 5c–d shows the response of the system under different MW pulses. Note that we took the quantization axis of the nuclear qubit to be along its local field when the electron spin was in the $m=-1$ state. MW_0 was the strongest pulse and was tuned in resonance with the transition between the centre spin states $|m=0\rangle$ and $|m=-1\rangle$, which was used to execute the centre spin flips in the DD sequence. The Rabi frequency of this control pulse was chosen to be 25 MHz, much larger than the hyperfine coupling strength (6.41 MHz), so that the electron spin flip was completed in a short time (<20 ns) and therefore was independent of the nuclear spin states. The other three MW channels used relatively weaker MW power so that the power broadening was less than the hyperfine splitting due to the nuclear qubit to selectively drive Rabi oscillations. MW_1 and MW_2 were tuned, respectively, resonant with the transitions $|0\downarrow\rangle \leftrightarrow |-1\downarrow\rangle$ and $|0\uparrow\rangle \leftrightarrow, |-1\uparrow\rangle$ so that they could be used to polarize and read out the nuclear spin state[34]. MW pulses were set to be about 1.25 MHz to selectively drive the $m_I=0$ component of the ^{14}N spin in the state tomography experiments, and were set to be about 4 MHz to drive all the ^{14}N spin components in the Ramsey interference experiments. The additional MW_3 channel was used for the 'kick out' pulses discussed below.

Polarization and readout of the nuclear qubit state. Figure 6a shows the polarization and readout schemes used to study the free precession of the target nuclear spin. As we encoded the centre spin qubit in the $m=0$ and $m=-1$ states, we enhanced the desired polarization by employing an extra MW channel (MW_3) to 'kick out' the unwanted component to the $m=+1$ subspace (Fig. 5b). For instance, to initialize the system to the $|0\downarrow\rangle$ state, the frequency of MW_3 was set to be in resonance with the transition $|0\uparrow\rangle \leftrightarrow |+1\uparrow\rangle$, and a π-pulse of this frequency was added after performing the initialization steps as in Gurudev Dutt *et al.*[33] This modification helped improve the effective polarization to 90% in the $m_I=0$ subspace.

In Fig. 6b,c, we show the effect of the 'kick out' pulse on polarization of the target nuclear spin. When the 'kick out' pulse was not applied, both MW_1 and MW_2 drove significant Rabi nutations, which indicates incomplete polarization (Fig. 6b). By using the MW_3, the unwanted components were removed (Fig. 6c), leaving a high polarization in the subspace spanned by $|m=0\rangle$ and $|m=-1\rangle$. As the decay of the population in the $m=+1$ subspace to the $m=-1$ and $m=0$ subspaces was negligible within the timescale of interest, we neglected the contribution of the $m=+1$ population, and the centre spin state was read out by normalizing the NV centre fluorescence signal with respect to the full Rabi oscillation driven by MW_0.

Determination of ω_0 and ω_1. As the hyperfine tensor characterizing the interaction between the centre spin and a nuclear spin is in general not known, we resorted to independent experimental methods to extract the value of $\omega_{0/1}$ of the target ^{13}C nuclear spin under varying magnetic field strength and orientation. To determine ω_0, we first initialized the system into the $|0\downarrow\rangle$ or the $|0\uparrow\rangle$ states. The nuclear qubit was then allowed to precess about ω_0 for a variable time t before its state was read out. This gave both the magnitude and the direction of ω_0. Similar procedures with initial states of $|1\downarrow\rangle$ or the $|1\uparrow\rangle$ and precession about ω_1 allow one to determine ω_1 (Supplementary Methods).

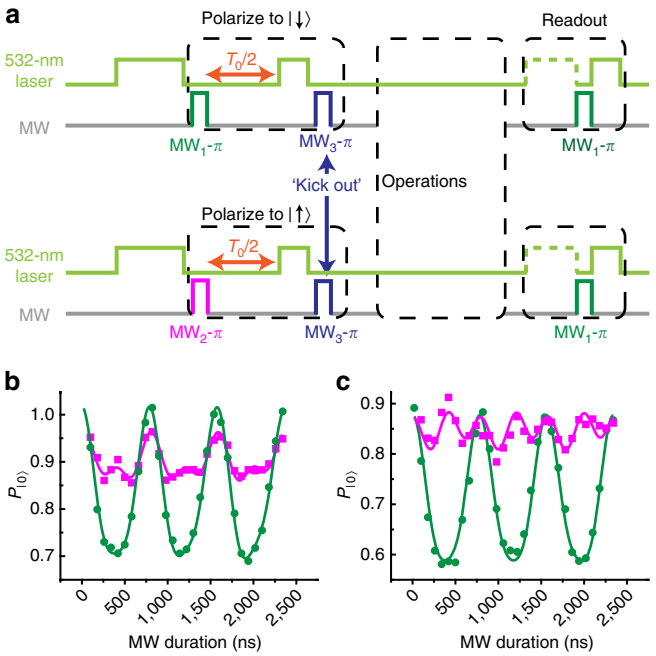

Figure 6 | Polarization and readout of the nuclear spin qubit. (**a**) Pulse sequence for polarizing and reading out the nuclear qubit. The polarization and readout schemes were adapted from the methods in Gurudev Dutt *et al.*[33], with an additional 'kick out' pulse to remove the unwanted population in the $|\uparrow\rangle$ state into the $m=+1$ subspace to increase the effective polarization. An additional 532-nm pulse was applied to initialize the centre spin if it was not in the $|0\rangle$ state before readout. (**b**,**c**) Selective Rabi oscillations driven by weak MW channels. The symbols are experimental data, and the lines are fitting to a superposition of two cosine functions corresponding to the in- and off-resonance oscillations. $P_{|0\rangle}$ denotes the population in the $|0\rangle$ state. (**b**) Polarizing the nuclear qubit to $|\downarrow\rangle$ without using the 'kick out' pulse. Large amplitude Rabi nutations driven by both MW_1 (green) and MW_2 (magenta) indicate that the polarization is incomplete. (**c**) Effect of the 'kick out' pulse. By employing the 'kick out' pulse, the population in the $|0\uparrow\rangle$ state is removed, and an effective polarization of 90% is achieved in the $m_I=0$ subspace. The residual oscillation driven by MW_2 is caused by the off-resonance excitation in the $m_I=\pm1$ subspaces, which also contributes as a dominant source of errors in the state tomography experiments.

State tomography. State tomography was performed by adopting the method detailed in Neumann *et al.*[51] using the transitions $|0\downarrow\rangle \leftrightarrow |1\downarrow\rangle$, $|0\uparrow\rangle \leftrightarrow |1\uparrow\rangle$ and $|0\uparrow\rangle \leftrightarrow |0\downarrow\rangle$ as the 'working transitions'. The first two transitions were driven by weak MW pulses, and the third one was realized by free precession of the nuclear qubit. The Rabi nutation and free precession signals were compared with the full oscillations in the $m_I=0$ subspace to extract the corresponding elements of the density matrix. The real and imaginary parts of the matrix elements were measured by using MW pulses with phases of 0 and $\pi/2$, respectively, and the required phase shift in the free precession signal was realized by transferring the populations to the $m=-1$ subspace and allowing the nuclear qubit to precess about ω_1. Other entries were obtained by transferring the corresponding populations to one of the working transitions. To map out all the off-diagonal elements, each of the diagonal elements in the density matrix was measured three times, and the data presented were taken as the mean of these measurements. The errors in the fidelity were calculated from the fitting errors of the Rabi nutations.

Sources of errors. In the experimental implementation of the scheme, a dominant source of errors originated from the imperfect selective π-pulses used. As the ^{14}N nitrogen spin was unpolarized in the experiment, the weak MW_1 and MW_2 channels, which were respectively used to drive selective Rabi oscillations between the $|0\downarrow\rangle \leftrightarrow |1\downarrow\rangle$ and $|0\uparrow\rangle \leftrightarrow |1\uparrow\rangle$ transitions in the $m_I=0$ subspace of the ^{14}N spin, would also partially drive the other ^{14}N-components. This resulted in imperfect selective π-pulses and limited the effective polarization to only 90% even after applying the 'kick out' pulse (Fig. 6c). This introduced errors in both the initialization of the system and the state tomography process.

Such imperfection, however, does not affect the performance of the DD gate as the scheme used only non-selective centre spin DD pulses. The Rabi frequency of the strong MW channel (MW_0) (25 MHz) was much higher than the hyperfine interaction strengths for both the ^{14}N and ^{13}C nuclear spins, and this allowed Rabi oscillation between $|0\rangle$ and $|1\rangle$ regardless of the states of the nuclear spins. Therefore, the fidelity of the demonstrated quantum gate should still be higher than that inferred from the measured state fidelities, which are currently limited by the errors in the weak selective MW pulses used in spin initialization and state tomography.

Design of DD gates by numerical optimization. We adopted a numerical optimization protocol similar to the one adopted in Khaneja *et al.*[52] for the optimization of the average two-qubit fidelity $\overline{F}\{t_\alpha\}$ subjected to the DD constraints (echo condition and symmetric sequence). In each optimization step, we updated $t_\alpha \rightarrow t_\alpha + \varepsilon \partial_{t_\alpha} \overline{F}$ subjected to the DD constraints, where $\partial_{t_\alpha} \overline{F}$ could be directly calculated by evaluating $\partial_{t_\alpha} U$ (Supplementary Methods) and ε is a small numerical parameter.

Simulation of the spin bath. The spin bath was simulated by considering the ^{14}N nitrogen host nuclear spin together with ^{13}C nuclear spins randomly placed in the diamond lattice with the natural abundance of 1.1%. Although the hyperfine coupling between the centre spin and the ^{14}N was modelled by established parameters, the coupling between the centre spin and the rest of the bath spins, as well as the coupling between bath spins, was assumed to be dipolar[30,44]. The simulated bath was selected to reproduce the value of T_2^* in FID experiment.

References

1. Kitaev, A. Y. Quantum computations: algorithms and error correction. *Russ. Math. Surv.* **52,** 1191–1249 (1997).
2. Terhal, B. M. & Burkard, G. Fault-tolerant quantum computation for local non-Markovian noise. *Phys. Rev. A* **71,** 012336 (2005).
3. Aharonov, D., Kitaev, A. & Preskill, J. Fault-tolerant quantum computation with long-range correlated noise. *Phys. Rev. Lett.* **96,** 050504 (2006).
4. Duan, L. M. & Guo, G. C. Preserving coherence in quantum computation by pairing quantum bits. *Phys. Rev. Lett.* **79,** 1953–1956 (1997).
5. Lidar, D. A., Chuang, I. L. & Whaley, K. B. Decoherence-free subspaces for quantum computation. *Phys. Rev. Lett.* **81,** 2594–2597 (1998).
6. Ban, M. Photon-echo technique for reducing the decoherence of a quantum bit. *J. Mod. Opt.* **45,** 2315–2325 (1998).
7. Viola, L. & Lloyd, S. Dynamical suppression of decoherence in two-state quantum systems. *Phys. Rev. A* **58,** 2733–2744 (1998).
8. Khodjasteh, K. & Lidar, D. A. Fault-tolerant quantum dynamical decoupling. *Phys. Rev. Lett.* **95,** 180501 (2005).
9. Yang, W., Wang, Z. Y. & Liu, R. B. Preserving qubit coherence by dynamical decoupling. *Front. Phys.* **6,** 2–14 (2011).
10. Biercuk, M. J. *et al.* Experimental Uhrig dynamical decoupling using trapped ions. *Phys. Rev. A* **79,** 062324 (2009).
11. Du, J. *et al.* Preserving electron spin coherence in solids by optimal dynamical decoupling. *Nature* **461,** 1265–1268 (2009).
12. de Lange, G., Wang, Z. H., Ristè, D., Dobrovitski, V. V. & Hanson, R. Universal dynamical decoupling of a single solid-state spin from a spin bath. *Science* **330,** 60–63 (2010).
13. Ryan, C. A., Hodges, J. S. & Cory, D. G. Robust decoupling techniques to extend quantum coherence in diamond. *Phys. Rev. Lett.* **105,** 200402 (2010).
14. Bluhm, H. *et al.* Dephasing time of GaAs electron-spin qubits coupled to a nuclear bath exceeding 200 μs. *Nat. Phys.* **7,** 109–113 (2011).
15. Bylander, J. *et al.* Noise spectroscopy through dynamical decoupling with a superconducting flux qubit. *Nat. Phys.* **7,** 565–570 (2011).
16. Viola, L., Lloyd, S. & Knill, E. Universal control of decoupled quantum systems. *Phys. Rev. Lett.* **83,** 4888–4891 (1999).
17. Souza, A. M., Álvarez, G. A. & Suter, D. Experimental protection of quantum gates against decoherence and control errors. *Phys. Rev. A* **86,** 050301(R) (2012).
18. West, J. R., Lidar, D. A., Fong, B. H. & Gyure, M. F. High fidelity quantum gates via dynamical decoupling. *Phys. Rev. Lett.* **105,** 230503 (2010).
19. Piltz, C., Scharfenberger, B., Khromova, A., Varón, A. F. & Wunderlich, C. Protecting conditional quantum gates by robust dynamical decoupling. *Phys. Rev. Lett.* **110,** 200501 (2013).
20. Cappellaro, P., Jiang, L., Hodges, J. S. & Lukin, M. D. Coherence and control of quantum registers based on electronic spin in a nuclear spin bath. *Phys. Rev. Lett.* **102,** 210502 (2009).
21. van der Sar, T. *et al.* Decoherence-protected quantum gates for a hybrid solid-state spin register. *Nature* **484,** 82–86 (2012).
22. Xu, X. *et al.* Coherence-protected quantum gate by continuous dynamical decoupling in diamond. *Phys. Rev. Lett.* **109,** 070502 (2012).
23. Ng, H. K., Lidar, D. A. & Preskill, J. Combining dynamical decoupling with fault-tolerant quantum computation. *Phys. Rev. A* **84,** 012305 (2011).
24. Khodjasteh, K., Lidar, D. A. & Viola, L. Arbitrarily accurate dynamical control in open quantum systems. *Phys. Rev. Lett.* **104,** 090501 (2010).
25. Khodjasteh, K., Bluhm, H. & Viola, L. Automated synthesis of dynamically corrected quantum gates. *Phys. Rev. A* **86,** 042329 (2012).
26. Witzel, W. M., Carrol, M. S., Cywiński, Ł. & Das Sarma, S. Quantum decoherence of the central spin in a sparse system of dipolar coupled spins. *Phys. Rev. B* **86,** 035452 (2012).
27. Yao, W., Liu, R. B. & Sham, L. J. Restoring coherence lost to a slow interacting mesoscopic spin bath. *Phys. Rev. Lett.* **98,** 077602 (2007).
28. Maze, J. R., Taylor, J. M. & Lukin, M. D. Electron spin decoherence of single nitrogen-vacancy defects in diamond. *Phys. Rev. B* **78,** 094303 (2008).
29. Zhao, N., Wang, Z. Y. & Liu, R. B. Anomalous decoherence effect in a quantum bath. *Phys. Rev. Lett.* **106,** 217205 (2011).
30. Huang, P. *et al.* Observation of an anomalous decoherence effect in a quantum bath at room temperature. *Nat. Commun.* **2,** 570 (2011).
31. Hodges, J. S., Yang, J. C., Ramanathan, C. & Cory, D. G. Universal control of nuclear spins via anisotropic hyperfine interactions. *Phys. Rev. A* **78,** 010303(R) (2008).
32. Khaneja, N. Switched control of electron nuclear spin systems. *Phys. Rev. A* **76,** 032326 (2007).
33. Gurudev Dutt, M. V. *et al.* Quantum register based on individual electronic and nuclear spin qubits in diamond. *Science* **316,** 1312–1316 (2007).
34. Jiang, L. *et al.* Repetitive readout of a single electronic spin via quantum logic with nuclear spin ancillae. *Science* **326,** 267–272 (2009).
35. de Lange, G., Ristè, D., Dobrovitski, V. V. & Hanson, R. Single-spin magnetometry with multipulse sensing sequences. *Phys. Rev. Lett.* **106,** 080802 (2011).
36. Maze, J. R. *et al.* Nanoscale magnetic sensing with an individual electronic spin in diamond. *Nature* **455,** 644–647 (2008).
37. Kolkowitz, S., Unterreithmeier, Q. P., Bennett, S. D. & Lukin, M. D. Sensing distant nuclear spins with a single electron spin. *Phys. Rev. Lett.* **109,** 137601 (2012).
38. Taminiau, T. H. *et al.* Detection and control of individual nuclear spins using a weakly coupled electron spin. *Phys. Rev. Lett.* **109,** 137602 (2012).
39. Zhou, N. *et al.* Sensing single remote nuclear spins. *Nat. Nanotechnol.* **7,** 657–662 (2012).
40. Childress, L. *et al.* Coherent dynamics of coupled electron and nuclear spin qubits in diamond. *Science* **314,** 281–285 (2006).
41. Nielsen, M. A., Dowling, M. R., Gu, M. & Doherty, A. C. Quantum computation as geometry. *Science* **311,** 1133–1135 (2006).
42. Nielsen, M. A. & Chuang, I. L. *Quantum Computation and Quantum Information* (Cambridge University Press, 2000).
43. Yang, W. & Liu, R. B. Quantum many-body theory of qubit decoherence in a finite-size spin bath. *Phys. Rev. B* **78,** 085315 (2008).
44. Zhao, N., Ho, S. W. & Liu, R. B. Decoherence and dynamical decoupling control of nitrogen vacancy center electron spins in nuclear spin baths. *Phys. Rev. B* **85,** 115303 (2012).
45. Nielsen, M. A. A simple formula for the average gate fidelity of a quantum dynamical operation. *Phys. Lett. A* **303,** 249–252 (2002).
46. Uhrig, G. S. Keeping a quantum bit alive by optimized π-pulse sequences. *Phys. Rev. Lett.* **98,** 100504 (2007).
47. Zanardi, P. Symmetrizing evolutions. *Phys. Lett. A* **258,** 77–82 (1999).
48. Viola, L., Knill, E. & Lloyd, S. Dynamical decoupling of open quantum systems. *Phys. Rev. Lett.* **82,** 2417–2421 (1999).
49. Wang, Z. Y. & Liu, R. B. Protection of quantum systems by nested dynamical decoupling. *Phys. Rev. A* **83,** 022306 (2011).
50. Souza, A. M., Álvarez, G. A. & Suter, D. Robust dynamical decoupling for quantum computing and quantum memory. *Phys. Rev. Lett.* **106,** 240501 (2011).
51. Neumann, P. *et al.* Multipartite entanglement among single spins in diamond. *Science* **320,** 1326–1329 (2008).
52. Khaneja, N., Reiss, T., Kehlet, C., Schulte-Herbrüggen, T. & Glaser, S. J. Optimal control of coupled spin dynamics: design of NMR pulse sequences by gradient ascent algorithms. *J. Magn. Reson.* **172,** 296–305 (2005).

Acknowledgements

This work was supported by National Basic Research Program of China (973 Program project Nos. 2009CB929103 and 2013CB921800), the National Natural Science Foundation of China (project Nos. 10974251, 11028510, 11227901, 1161160553 and 91021005), Hong Kong Research Grants Council—National Natural Science Foundation of China Joint Project N_CUHK403/11, the Chinese University of Hong Kong Focused Investments Scheme and Hong Kong Research Grants Council—Collaborative Research Fund Project HKU8/CRF/11G.

Author contributions

R.-B.L. proposed the project and conceived the idea. H.C.P. designed the scheme and carried out the theoretical study. X.-Y.P. and G.-Q.L. designed the experiment. G.-Q.L.

carried out the experimental study. H.C.P. and G.-Q.L. wrote the paper. J.D. discussed the scheme and the results. All authors analysed the data and commented on the manuscript.

Additional information

Supplementary Information accompanies this paper at http://www.nature.com/naturecommunications

Competing financial interests: The authors declare no competing financial interests.

Reprints and permission information is available online at http://npg.nature.com/reprintsandpermissions/

How to cite this article: Liu, G.-Q. *et al.* Noise-resilient quantum evolution steered by dynamical decoupling. *Nat. Commun.* 4:2254 doi: 10.1038/ncomms3254 (2013).